Biochimica et Biophysica Acta, 1109 (1992) 141–148

BBAMEM 75733

Quantitation of physical-chemical properties of the aqueous phase inside the phoE ionic channel

M. Gutman [a], Y. Tsfadia [a], A. Masad [b] and E. Nachliel [a]

[a] *Laser Laboratory for Fast Reactions in Biology, Department of Biochemistry, The George S. Wise Faculty of Life Sciences, Tel Aviv University, Tel Aviv (Israel) and* [b] *School of Chemistry, The Raymond and Beverly Sackler Faculty of Exact Sciences, Tel Aviv University, Tel Aviv (Israel)*

(Received 31 March 1992)

Key words: phoE ion channel; Water filled channel; Aqueous phase; Ionic channel

The anion-specific channel of the phoE porine is a miniature body of water surrounded by peptide walls. The physical and chemical properties of the water in such a microscopic space were measured by monitoring the dynamics of a well-studied reaction – the protolytic dissociation of a strong acid. To attain this purpose, we allowed pyranine (8-hydroxypyrene-1,3,6-trisulfonate) to bind to the anion-specific channel. The dye is bound, with a 1:1 stoichiometry, with a $\Delta G = -9.5$ kcal/mol. Photoexcitation of the dye, to its first electronic singlet state (ΦOH^*), renders it very acidic and the hydroxyl proton dissociates to H^+ and excited anion (ΦO^{*-}). We employed single photon-counting time-resolved fluorimetry, to monitor the reversible dissociation of pyranine as it proceeds within the channel and reconstructed the observed signal by a numerical integration of the differential diffusion equation pertinent for a proton within the channel. The most characteristic feature of the water-filled channel, is the intensified electrostatic interactions attained by the low dielectric constant of the diffusion space, $\epsilon_{eff} = 24$. For this reason, the electric field of a few positive charges is sufficient to ensure that an anion entering the channel will be effectively sucked in. The interaction of the water molecules with the peptide structure forming the channel affects the physical properties of the water. Their capacity to conduct proton, quantitated by the protons diffusion coefficient ($4.5 \cdot 10^{-5}$ cm^2/s), is reduced by 50% with respect to that of bulk water. The activity of the water in the channel is reduced to $a_{H_2O} = 0.966$. These observation are in accord with our previous studies of water in small defined cavities in proteins.

Introduction

Cell membranes are made to be selective boundaries, allowing a controlled influx of solutes. To attain this goal, the lipid component of the membranes forms an impermeable barrier, while pore proteins or pumps provide the selective gates. The porines [1,2], the pore proteins of the outer membrane of the Gram-negative bacteria, are a common and convenient model for the study of large transporting channels that cross lipid membrane.

The phoE porine of *E. coli* is an anion-selective channel functioning, under physiological conditions, as an inlet for phosphate or phosphosugars [3]. The protein is well-studied and the structure of the pore is known [4]. It appears as a trimer, where each unit consists of a funnel shaped pore. At the outer side of the membrane, the pore is large, elliptical in shape, and measures 27 Å × 17 Å. On the inner side of the membrane it is much narrower, only 10 Å. Within the pore there are 12 positive amino acid residues and 9 carboxylates [3]. The electrostatic potential of the net space charge (+3) is further amplified by the dielectric boundary between the water in the pore and the low dielectric matrix of the β-plated sheets which form the walls of the pore [5,6].

The passage of ions through channels is usually monitored by steady-state current or flux measurements [7], which per definition cannot provide a dynamic information of the ion passage. That higher level of understanding requires a time-resolving element in measurement like the frequency spectrum of the conductivity [8]. In the present communication, we wish to describe another time-resolved methodology for the study of ion passage in a channel; a real time-monitoring of a single ion diffusing within the channel and its interaction with a molecular probe located within the same channel.

The time-resolved technique we use is the Laser Induced Proton Pulse [9], where a picosecond light

Correspondence to: M. Gutman, Laser Laboratory for Fast Reactions in Biology, Department of Biochemistry, The George S. Wise Faculty of Life Sciences, Tel Aviv University, Ramat Aviv 69978, Tel Aviv, Israel.

pulse is used to excite a molecule of pyranine (8-hydroxypyrene-1,3,6-trisulfonate) to its first electronic singlet state (ΦOH^*). In this state the dye is very acidic and ejects the hydroxyl's proton with a time constant of approx. 100 ps. Time-resolved fluorometry monitors the dissociation of the dye and numerical analysis of the signal provides detailed information about the matrix in which the reaction takes place [10–12]. This methodology was previously used for gauging the properties of water in concentrated solutions of sucrose [13], in microscopic cavities in a protein [14] or the interbilayer space of multilamellar vesicles [15].

In the present case, we exploited the high affinity of the phoE channel for anions to form a stable complex between the purified protein and pyranine. Excitation of the dye produces an ion pair (H^+ and ΦO^{*-}) within the channel and subnanosecond measurements monitor how the proton either evicts the channel or alternatively recombines with ΦO^{*-}. A numeric analysis of the observed, time-resolved fluorescence could reconstruct the experimental observation with high accuracy. By this procedure we quantitated the effective dielectric constant of the aqueous phase within the channel ($\epsilon = 24$) and the diffusion coefficient of proton ($D_{H^+} = 4.5 \cdot 10^{-5}$ cm^2/s). The dynamic characteristics of a substrate molecule within the channel is presented.

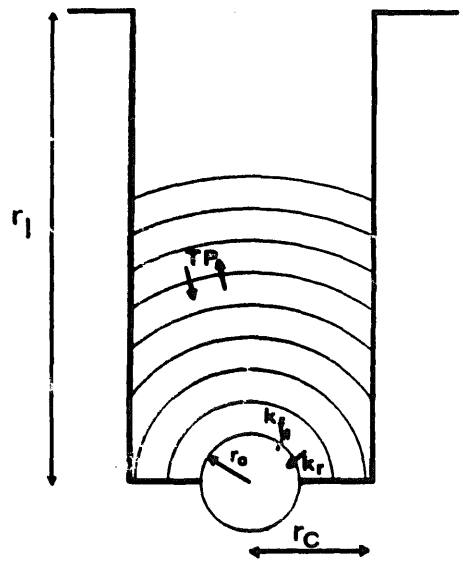

Scheme 1. Schematic description of the phoE channel used for analysis of the experimental observation. The pyranine, represented by a sphere $r_0 = 6$ Å, is placed at the bottom of the wide section of the channel. The channel itself behaves as a single open cylinder with $r_c = 14$ Å and a length $r_l = 43$ Å. The proton appears at the surface of r_0 with a rate constant k_f and is re-adsorbed at a rate k_r. The diffusion of the proton is a series of consecutive steps between concentric shells, each with a width Δr. The probability of passage between two shells (TP given in s^{-1} units) is determined by the electrochemical gradient between the shells. A proton reaching the mouth of the channel ($r_i = r_l$) is assumed to be irreversibly lost to the bulk.

Materials and Methods

Purified phoE protein was a generous gift from J. Tommassen, Department of Molecular Cell Biology, State University of Utrecht, The Netherlands. Pyranine laser grade, was purchased from Kodak. Detergents, SDS and Brij 58, were from Sigma.

Binding of pyranine to phoE. The protein was dissolved in 1% SDS + 1.1% Brij 58 to final concentration of 50 μM. The solution was dialyzed against 250 μM pyranine dissolved in the same detergents at pH 5.5. After 24 h equiiibration, excess of dye and SDS were removed by dialysis against 1.4% Brij 58. The final protein preparation was approx. 70% complexed with the dye, while the free dye concentration was less than 0.1% of the total.

Steady state fluorometry was measured with a Shimadzu RF540 spectrofluorometer. Time-resolved fluorescence was measured with 20-μl samples of dye-protein complex containing approx. 30 μM dye. The instrumental setup for the time-resolved fluorescence consisted of a mode-locked Nd-Yag laser, pumping a cavity damped dye laser followed by frequency doubling ($\lambda = 300$ nm). The fluorescence of ΦOH^* was monitored by single photon counting. More details are given in the experimental paper of Huppert and his colleagues [16].

The analysis of the fluorescence decay of ΦOH^* emission was carried out by the computer program written by Agmon [10–12] which recreates the observed signal by numerical reconstruction of the process. The reconstruction incorporates two interdependent mechanisms: (1) The chemical reaction at the surface of the reaction sphere, characterized by dissociation (k_f) and recombination (k_r) at the distance r_0 (see Scheme I). (2) The diffusion of the proton within the electrostatic field of the anion. The diffusion is envisioned as a set of consecutive stepping of the proton between concentric shells (Δr each), where the probability of stepping $TP_{i/j}$ is given by Eqn. 1:

$$TP_{i/j} = \frac{D_{H^+}}{\Delta r^2} \cdot f^{(n)}\left(\frac{r_i}{r_j}\right) \cdot \exp\left[-\frac{R_D}{2}\left(\frac{1}{r_i} - \frac{1}{r_j}\right)\right] \qquad (1)$$

The first term in Eqn. 1 states that the diffusion coefficient (D_{H^+}) controls linearly the frequency of the transitions. The second term states that a particle will prefer to diffuse into a shell which provides it with a larger volume. For a diffusion in a three-dimensional space, the value of $f^{(3)}_{(r_i/r_j)}$ is r_i/r_j, while for a one-dimensional space the function equals unity ($f^{(1)}_{(r_i/r_j)} = 1$).

The last term in Eqn. 1 denotes the gradient of the electrostatic pair potential. R_D in this equation (the Debye radius) is the distance at which the dielectrics of

the diffusion medium reduce the electrostatic pair potential to the level of thermal energy. From this parameter (R_D), we extract the effective dielectric constant averaged for the whole volume probed by the proton.

$$\epsilon_{eff} = Z_1 Z_2 e_0^2 / R_D kT \quad (2)$$

In the present case, where the diffusion proceeds in a space confined by boundaries that temporarily retain the proton, the program includes the reversible interaction of the proton with the boundary's proton binding elements. The diffusion space is taken as three-dimensional, up to $r_i = r_c$. At longer distance $r_i > r_c$ the diffusion space was taken as one-dimensional. The reversible association with the walls of the channel was taken to be constant over the whole space, independent of the proton's position. A proton which reached the end of the channel $r_i = r_l$ is irreversibly diluted in the bulk.

The computer program combines the chemical reactions at r_0 and the diffusion process (given by Eqn. 1) into a Master Equation with detailed balance and propagates it in time to regenerate the probability density of the proton over time and space using the Chebishev expansion method.

Results and Discussion

Binding of pyranine to phoE protein

Binding of pyranine to the phoE protein was measured by equilibrium dialysis. The protein (50 μM) was dissolved in a solution containing 1% SDS and 1.1% Brij 58. The protein was equilibrated by dialysis against varying concentrations of pyranine dissolved in the same solution. After 24 h of equilibration, the dye concentrations on both sides of membrane was determined. The dye in the bathing solution was taken as equal to the free dye in the bag, while any excess above that was equated with the protein-bound dye.

The binding of the dye to the protein corresponds to a 1:1 complex with $K_{as} = 1.2 \cdot 10^4$ M. Removal of the anionic detergent increases the association constant to $K_{as} = (7.8 \pm 0.2) \cdot 10^6$ M.

The pK of the dye in the complex (p$K = 7.7 \pm 0.05$), measured at low ionic strength ($I = 0.004$) is similar to that measured either in water or in Brij 58.

The binding of the dye is reversible. Dialysis against 100 mM Na_2SO_4 removes the dye completely.

Fluorescence of dye-protein complex

The steady-state fluorescence emission of pyranine is shown in the insert to Fig. 1. The emission consists of two bands, a weak emission at 450 nm, where ΦOH* fluoresces and an intensive band at 515 nm, where ΦO^{*-} emits. As the fluorescence lifetime of both forms (ΦOH* and ΦO^{*-}) are almost the same, 6-and 5.5 ns respectively, the enhanced emission of ΦO^{*-} implies that most of the excited dye ejects its proton before decaying to the ground state.

The rapid dissociation of the proton from ΦOH* is directly observed by the time-resolved fluorimetry shown in Fig. 1. The dye was excited by a 1 ps laser pulse and its emission was monitored at the wavelength

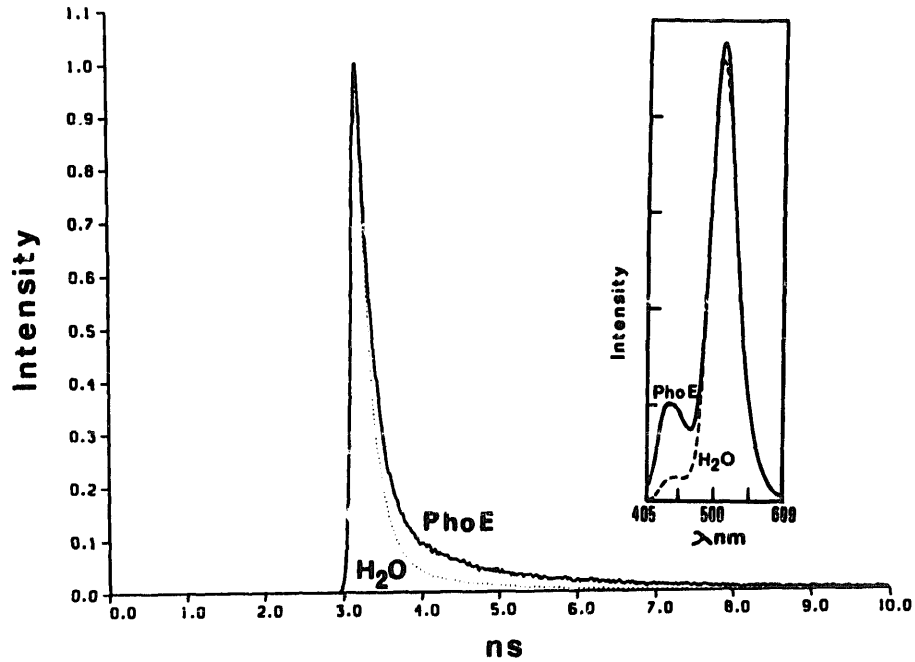

Fig. 1. Comparison between the fluorescence of free pyranine and the phoE pyranine complex. The main frame depicts the time-resolved emission of the excited form of the protonated dye (ΦOH*) ($\lambda = 430$ nm). The inset depicts the steady-state fluorescence of the dye (excitation at 390 nm). The measurements were carried out at pH 5.5 using 50 μM of free or protein-bound dye.

of ΦOH* emission. The fluorescence intensity decays very rapidly in an almost exponential curve down to approx. 5% of initial intensity. From there on, the decay is much slower. This long fluorescence 'tail' is the mark of geminate recombination, a process whereby the just ejected proton recombines with ΦO^{*-} to reproduce the parent molecule ΦOH* [10–12]. The same features are found in the fluorescence of the porine-dye complex, where the ΦOH* emission is intensified both in the steady-state and the time-resolved domain (see Fig. 1).

The enhancement of the geminate recombination process is attributed to the confining walls of the proteinaceous structure [14,17] where the impenetrable walls and the intensified electrostatic potential retain the proton within the close proximity of ΦO^{*-}.

Kinetic analysis of geminate recombination in the ion channel

The model used for analysis of the observed dynamics is presented in Scheme I. The channel is depicted as a cylindrical cavity within a low dielectric, proton impermeable, matter. The pyranine is placed inside the cavity and the ejected proton diffuses in hemispherical symmetry until $r_i = r_c$. Within this range the value of $f(r_i/r_j)$ (Eqn. 1) is r_i/r_j. At a longer distance ($r_i > r_c$) the proton propagates in a tube. For this geometry the diffusion space is approximated by a one-dimensional space and the $f(r_i/r_j)$ in Eqn. 1 is taken as unity. A proton coming to the end of the channel is diluted and irreversibly lost to the bulk. Re-entry of proton from the bulk, within the observation period, has a negligible probability.

Within the channel, the electrostatic interactions are attenuated by an effective dielectric constant ϵ_{eff} which is the average value over the whole space.

The parameters used for the simulation were: k_f and k_r, which quantitate the chemical reaction on the surface of the reaction sphere (r_0). The diffusion coefficient D_{H^+}, the effective dielectric constant ϵ_{eff} and the rate of proton binding to the surface groups (k_{as}).

The computer program was fed with first estimates of these variables, a simulated dynamics was generated, compared with the experimental one and the variables were adjusted to obtain the best fit of the theoretical line with respect to experimental tracing. The theoretical fitting of the experimental curve is shown in Fig. 2 on a linear and a logarithmic Y scale. The former is a better presentation for the initial phase of the dynamics, the latter demonstrates the quality of the fit at the lower range of the scale. The parameters needed to gain this fit are listed in Table I.

As more than one variable was adjusted to gain the high-quality fit shown in Fig. 2, it is of interest to investigate how each variable modulates the shape of the dynamic curve (see Fig. 3).

On drawing (A) of Fig. 3, we varied the rate of proton dissociation at the surface of the reaction

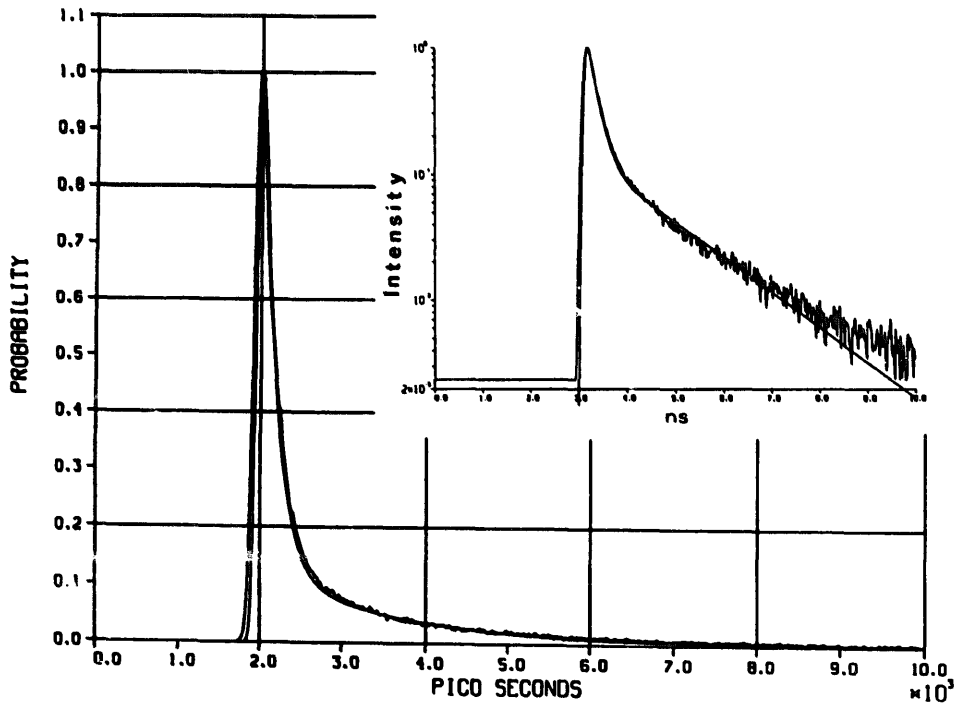

Fig. 2. Theoretical reconstruction of the observed signal of the time-resolved fluorescence of the protein-dye complex. The main frame depicts the observed signal (as shown in Fig. 1) with the superpositioned dynamics generated by numerical simulation using the parameters listed in Table I. The inset depicts the same data using a logarithmic scale in order to demonstrate the accuracy of the fit down to 1% of the initial amplitude.

TABLE I

The physical properties of the aqueous phase in the phoE anionic channel and the reaction parameters characterizing the reaction of a proton in the channel

	Channel	Water
Effective dielectric constant	24 ±1	78
Diffusion coefficient (cm^2/s)	$4.5 \pm 0.5\ 10^{-5}$	$9.3\ 10^{-5}$
a_{H_2O}	0.966	1.000
Rate of dissociation (k_f) from ΦH^* (s^{-1})	$5.5 \pm 0.5\ 10^9$	$7 \pm 0.2\ 10^9$
Rate of recombination (k_r) with ΦO^{*-} (A/s)	$4.3 \pm 0.2\ 10^9$	$7 \pm 0.3\ 10^9$
Rate of reaction with protonable moieties on the channel's wall (s^{-1})	$7 \pm 0.5\ 10^8$	*n.a.* [a]

[a] Not applicable.

sphere. When this reaction is fast, the dynamics exhibit a clear distinction between the fast initial decay and the shallow tail. As the dissociation is slowed, the initial decay is milder and merges more smoothly with the slower phase. It must be stressed that, of all reaction parameters, k_f is the only one affecting the dynamics from zero time. All other parameters modulate the amplitude of the slow phase, its point of initiation or the curvature of the transition (compare frames B–D, Fig. 3).

(B) in Fig. 3, depicts the effect of the attenuation of the electrostatic potential by the dielectric constant of the channel space. At high dielectric environments the amplitude of the tail is small, corresponding with high probability of the proton to escape out of the electric attraction of the ion. A low dielectrics of the channel

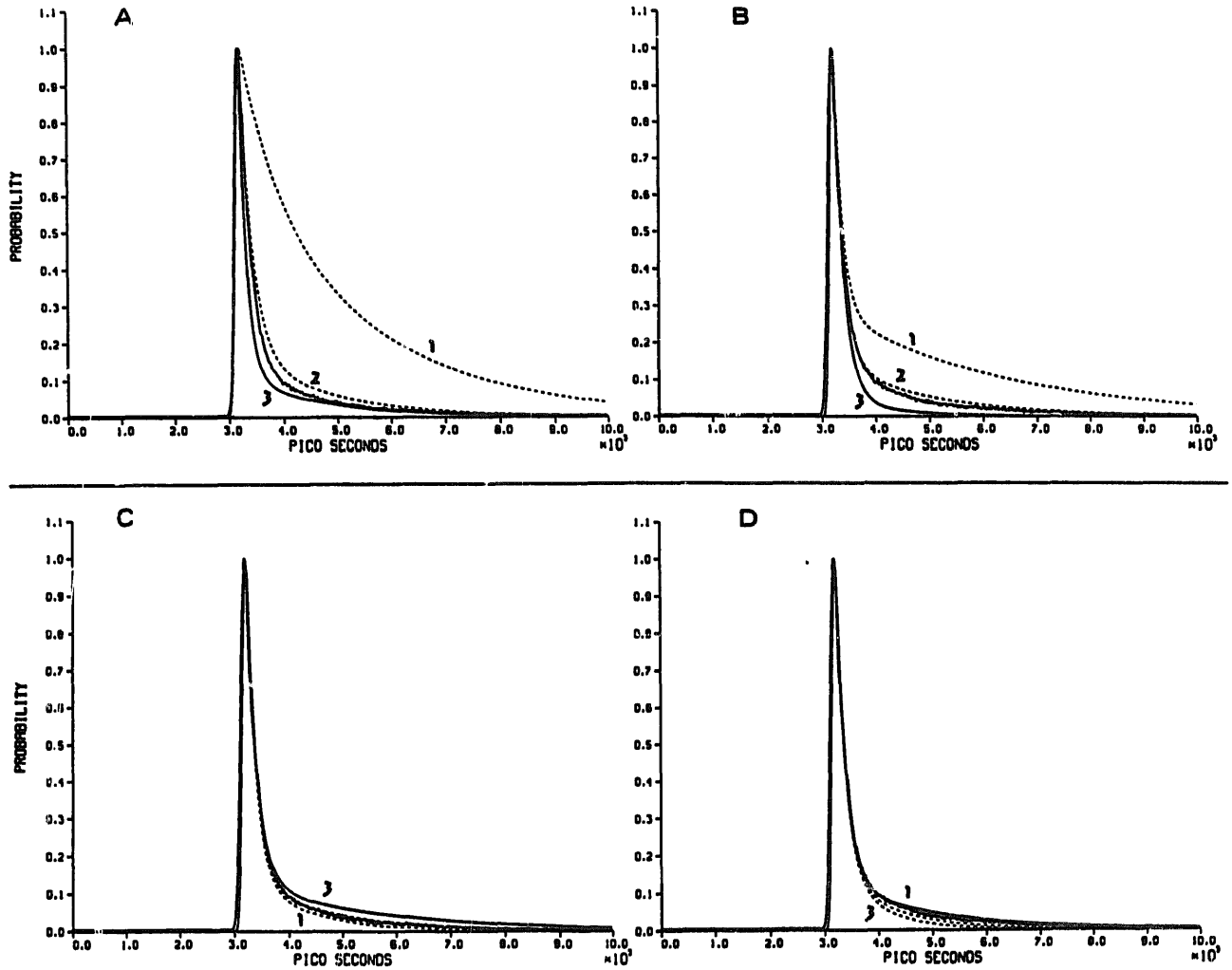

Fig. 3. The effects of the reaction parameters on the shape of the theoretically reconstructed dynamics. Each frame in this figure depicts the experimental signal plus three simulated curves where a single reaction parameter is varied: (A) The rate of proton dissociation $k_f = 7 \cdot 10^7$ (line 1); $3.8 \cdot 10^9$ (line 2) and $7 \cdot 10^9$ (line 3); (B) The effective dielectric constant assumes the values of 5 (1); 30 (2) and 78 (3); (C) The diffusion coefficient of the proton, D_{H^+} equals $9.3 \cdot 10^{-5}$ (1) $4.5 \cdot 10^{-5}$ (2) and $2 \cdot 10^{-5}$ (3). Curve 2 is superpositioned over the experimental curve and for clarity it is not marked; and (D) The rate of proton binding to the protonable moieties within the channel, k_{as} is equal to zero (1), $3.5 \cdot 10^8$ (2) and $7 \cdot 10^8$ (3).

space increases the magnitude of the tail, signifying that the proton is attracted to the anion over a larger section within the channel.

(C) in Fig. 3 depicts the effect of the diffusion coefficient of H^+. It is obvious from this drawing that D_{H^+} affects mostly the tail region. During the first phase, where the protons are still in the immediate vicinity of ΦO^{*-}, the recombination is almost insensitive to D_{H^+}. About 1 ns after dissociation, when protons are more dispersed in space, the effect of D_{H^+} is more distinct. Slow diffusion suppresses the dispersion of H^+ and the proton concentration close to ΦO^{*-} dwindles more slowly. Thus the probability of ΦOH^* reformation is higher in low D_{H^+} system. The experimental curve is best reconstructed with $D = 4.5 \cdot 10^{-5}$ cm^2/s.

In (D), we present the effect of the rate of proton binding to protonable moieties in the channel. This reaction modulates the dynamics mostly at the initial phase of the tail.

The four frames of Fig. 3 demonstrate that each of the variables affects the shape of the theoretical dynamics in a quite specific manner. Because of the specificity of variables and the complexity of the observed signal, we are convinced that the combination of parameters which reproduces the experimental curve (see Fig. 2 and Table I) is unique.

Spatio-temporal distribution of a proton in the ionic channel

The computation algorithm which so accurately reconstructed the dynamics of ΦOH^* population also produces the temporal distribution of the proton over the whole reaction space.

Fig. 4 depicts the probability of finding a proton in four locations, bound to the pyranine anion (curve A); a free proton in the channel (curve B); protons which diffused from the channel to the bulk (curve C) and those stuck on the channel's wall (curve D). The appearance of free protons in the channel is very fast (see curve B). About 0.5 ns after excitation, the probability density of free protons in the channel starts to decline. Two processes are responsible for that effect: diffusion of protons to the bulk and reversible trapping by protonable groups. Of these two, the escape to the bulk is the major pathway. Proton appears in the bulk within the first nanosecond (see curve C), indicating how fast a proton can run along the channel. Yet, it must be explicitly clear that this rapid motion is not due to any enhanced diffusion mechanism; it is a simple consequence of the small dimension of the channel. About 10 ns after the pulse, the only protons in the channel are bound to the carboxylates. These groups with pK 4–5, will retain the proton for a few microseconds [9], a time frame much longer than our fluorometric observation window.

A temporal distribution of free protons along the length of the channel is given in Fig. 5. The ordinate is the probability of finding a proton at any distance from the anion (right side abscissa) at any given time (left side abscissa). The protons appear at $t = 0$ on the surface of the reaction sphere and rapidly disperse up to $r_t = r_c$, driven by the expanding volume of the concentric shells. From that point onwards (see arrow

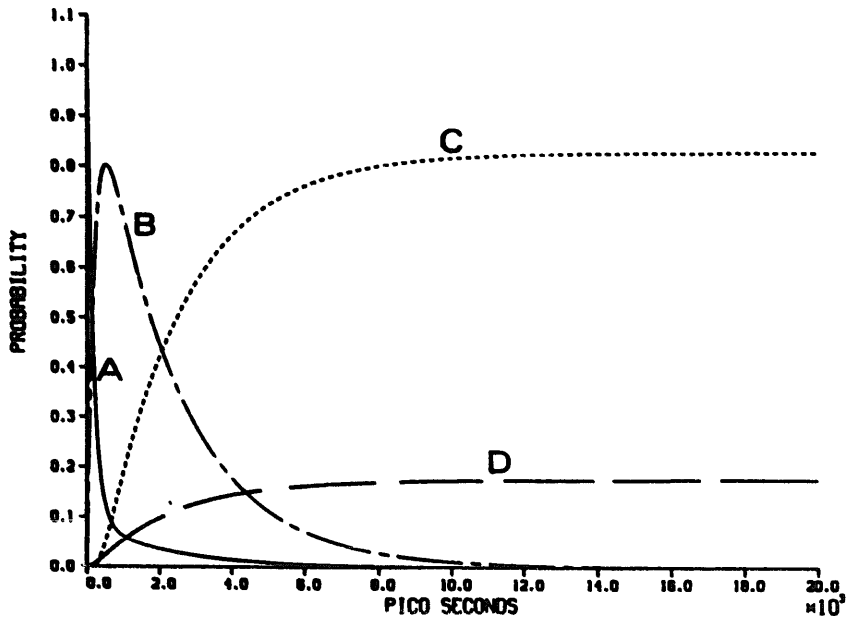

Fig. 4. The temporal distribution of protons in the phoE ion channel following photoexcitation of the dye. The curves correspond with; (A) The probability of finding a proton bound to the excited pyranine (ΦOH^*); (B) a free proton within the channel; (C) free proton in the bulk phase; and (D) Proton bound to the protonable carboxylates in the channel. The four curves correspond with the simulation dynamics shown in Fig. 2.

markings on the figure) the diffusion is along a tube, where the volume increment is not an attractor. Indeed in this region the decay of the probability density is less steep. The protons reach the edge of the channel in 0.5 ns, and as we see from Fig. 4, leak out with a time constant of approx. 2 ns. During the time when the protons leak out, highest proton concentration is very close to the anion, reflecting the intensive electrostatic attraction which prevents their homogeneous dispersion within the ionic channel. These calculations demonstrate a basic property of an ion in a channel. In spite of the fact that it vacates the cavity in a very short time, the distribution within the space is not homogeneous. The probability density of the proton follows the electrostatic potential profile within the microscopic space.

The analytic procedure which reconstructs the propagation of a proton in the channel can also simulate the diffusion of anion in the channel (see Fig. 6). In this figure we ascribe to the mobile species a charge of $Z = -2$ (as for phosphosugar) and a diffusion coefficient of a molecule of comparable size ($D = 1 \cdot 10^{-5}$ cm^2/s). The channel charge was taken as $Z = +3$ (the excess of positive charges in the channel) placed, for the sake of computation, at the same site we ascribed for the pyranine bound to the porine.

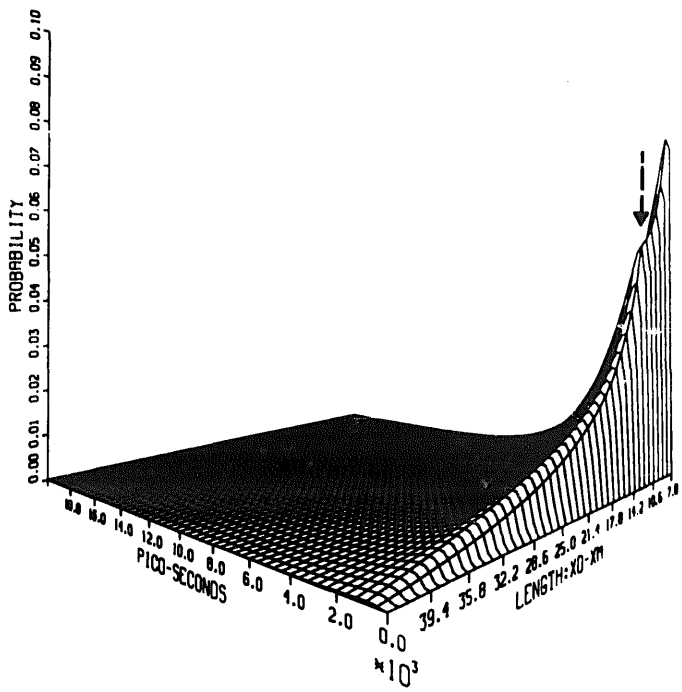

Fig. 5. The spatio-temporal distribution of free protons in the channel following excitation of the dye. The ordinate denotes the probability of finding a proton at a given time (marked on the left side abcissa) along the ionic channel (given by the right side abcissa). The proton appears in the innermost concentric shell (see Scheme I) and diffuses towards the mouth of the channel. The arrow marks the radial distance $r_t = r_c$, where the diffusion assumes a one-dimensional space regime. The data correspond with those given in Fig. 4.

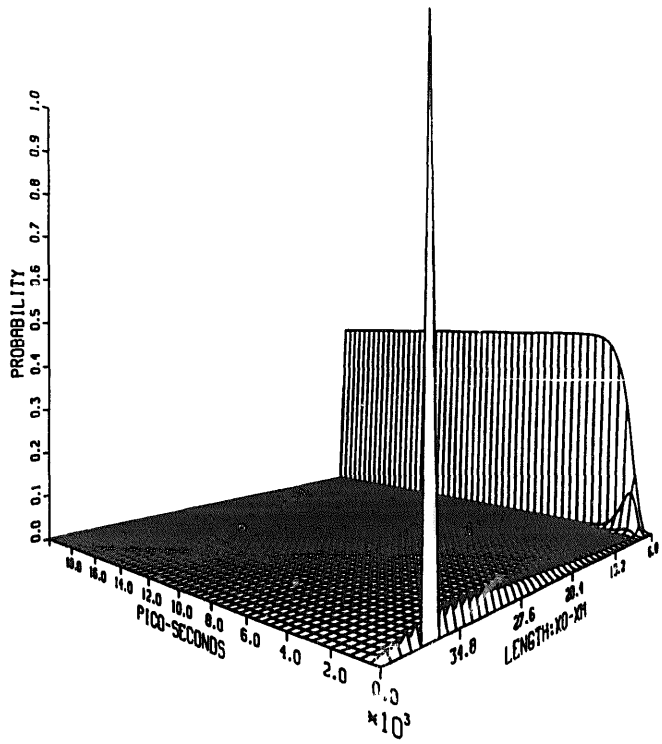

Fig. 6. Spatio-temporal distribution of anion entering the mouth of the channel. In this simulation, we exhibit the motion of anion like phosphosugar with $Z = -2$ and $D = 1 \cdot 10^{-5}$ cm^2/s. The simulation begins from the moment the ion entered the channel by full length of its radius, appearing at the spike at $t = 0$ in $r = 39$. With progress of time, the ion accumulates at the bottom of the channel, reaching 50% probability within approx. 2 ns. The rest of the anions leak out, as seen by the shallow ridge leading out.

The simulation was initiated from the time the substrate got into the channel by a full length of its radius. Within less than 2 ns, the anion diffuses the full length of the channel accumulating at the bottom of the well. The efficiency of that 'sucking in' process is high; approx. 50% of the molecules entering the mouth of the channel will end by going through it. Considering the fact that an ion at the mouth executes a Brownian motion which takes it in and out, then within a few random entries the probability of the substrate molecule to remain outside the channel will dwindle to zero.

The high efficiency at which the channel shuttles any anion that entered, has a straightforward mechanistic implication; the overall process becomes a diffusion-controlled reaction determined by the electrostatic field at the mouth of the channel [18]. Indeed, a single mutation replacing Lys-125 by glutamate suffices to revert the selectivity of the mutants phoE porine [19].

The dielectric constant of the space within the ion channel

The intensity of the electrostatic force, in the absence of ionic screening, is determined by the dielectric constant of the environment. For a homogeneous

medium, the dielectric constant is the same all over the space and its magnitude is directly related to the molecular properties of the matter. Near a dielectric discontinuity like membrane/water or protein/water interface, the dielectric constant is a function of the place, varying sharply as the test charge approaches the interface [20,21]. In the present case the proton probes the whole space and the dielectric constant we measured is the average of all local values. The measured dielectric constant, $\epsilon_{eff} = 24$, is much lower than of bulk water. This local value intensifies the electrostatic forces within the channel by a factor of approx. 3. Thus a small number of charges suffice to endow the channel with its high efficiency.

Properties of water within the channel

Very close to protein, water molecules may achieve a high degree of ordering, up to a state that they can be resolved in the X-ray diffraction pattern. Ordered water, influenced by strong interaction with the protein, may be less available for chemical reactions which require their rotation or translation.

Both proton dissociation and its diffusion in water require a rapid orientation of the solvent molecules around the charge of the proton [22]. Indeed, we find that these two parameters are suppressed within the channel, compared with the values measured in bulk water. Similar results were also obtained for the heme binding site of apomyoglobin [14] and the *N*-terminal region of lysozyme [17]. These observations corroborate molecular dynamic simulations that predict ordering of water at the protein surface [23].

This study might point to a general feature common to small aqueous cavity in a protein: the enclosed water molecules gain a higher degree of ordering. Thus, among the special properties of an active site of a protein, one should add another feature, the nonbulk property of the water in it.

Acknowledgement

This research is supported by the Office of Naval Research, U.S. Army grant No. N00014-89-J-1622.

References

1 Lautenberg, B. and Alphen, L.V. (1983) Biochim. Biophys. Acta 737, 51–115.
2 Benz, R. and Bauer, R. (1988) Eur. J. Biochem. 176, 1–19.
3 Ley, P.V.D. and Tommassen, J. (1987) in Phosphate Metabolism and Cellular Regulation in Microorganisms (Torrini- Gorini, M. et al., ed.) Publication of the American Society for Microbiology, p. 159.
4 Jap, B.K. (1989) J. Mol. Biol. 205, 407–419.
5 Jordan, P.C., Bacquet, R.J., McCammon, J.C. and Tran, P. (1989) Biophys. J. 55, 1041–1052.
6 Levitt, D.G. (1985) Biophys. J. 48, 19–31.
7 Benz, R. (1987) Crit. Rev. Biochem. 19, 145–190.
8 Läuger, P. (1987) Physiol. Rev. 67, 1296–1331.
9 Gutman, M. (1984) Methods Biochem. Anal. 30, 1–103.
10 Pines, E., Huppert, D. and Agmon, N. (1988) J. Chem. Phys. 88, 5610–5630.
11 Agmon, N. (1988) J. Chem. Phys. 88, 5639–5642.
12 Agmon, N. and Szabo, A. (1990) J. Chem. Phys. 91, 5270–5284.
13 Gutman, M., Nachliel, E. and Kiryati, S. (1992) Biophys. J., in press.
14 Shimoni, E., Tsfadia, Y., Nachliel, E. and Gutman, M., in Eletron Proton Transfer in Chemistry and Biology (Muller, A., ed.), Elsevier, Amsterdam, in press.
15 Gutman, M., Nachliel, E. and Kiryati, S. (1992) Biohpys. J., in press.
16 Huppert, D., Pines, E. and Agmon, N. (1990) J. Opt. Soc. Am. (B) 7, 1545–1560.
17 Yam, R., Kiryati, S., Nachliel, E. and Gutman, M. (1992) in NATO ASC on Electrified Interfaces in Physics, Chemistry and Biology (Guidelli, R., ed.), Kluwer, Dordrecht, in press.
18 Jordan, P.C. (1986) in Ion Channel Reconstitution (Miller, C., ed.), pp. 37–55, Plenum Press, New York.
19 Bauer, K., Struyre, M., Bosch, D., Benz, R. and Tommassen, J. (1989) Biol. Chem. 264, 16393–16398.
20 Gilson, M.K., Rashin, A., Fine, R. and Honig, B. (1985) J. Mol. Biol. 183, 503–510.
21 Cevc, G. (1990) Biochim. Biophys. Acta 1031, 311–382.
22 Gutman, M. and Nachliel, E. (1990) Biochim. Biophys. Acta 1015, 391–414.
23 Green, M.E. and Lewis, J. (1991) Biophys. J. 59, 419–426.